HerMES: Lyman Break Galaxies Individually Detected at $0.7 \leqslant z \leqslant 2.0$ in GOODS-N with *Herschel*/SPIRE

Denis Burgarella[1], Véronique Buat[1], Georgios Magdis[2] and the HerMES team

[1]Laboratoire d'Astrophysique de Marseille, OAMP, Université Aix-Marseille, CNRS, 38 rue Frédéric Joliot-Curie, 13388 Marseille cedex 13, France
email: `denis.burgarella@oamp.fr, veronique.buat@oamp.fr`

[2]Laboratoire AIM-Paris-Saclay, CEA/DSM/Irfu - CNRS - Université Paris Diderot, CE-Saclay, pt courrier 131, F-91191 Gif-sur-Yvette, France
email: `georgios.magdis@cea.fr`

Abstract. As part of the *Herschel* Multi-tiered Extragalactic Survey we have investigated the rest-frame far-infrared (FIR) properties of a sample of more than 4800 Lyman Break Galaxies (LBGs) in the Great Observatories Origins Deep Survey North field. Most LBGs are not detected individually, but we do detect a sub-sample of 12 objects at $0.7 < z < 1.6$ and one object at $z = 2.0$. The LBGs have been selected using color-color diagrams; the ones detected by *Herschel* SPIRE have redder colors than the others, while the undetected ones have colors consistent with average LBGs at $z > 2.5$. The spectral energy distributions of the objects detected in the rest-frame FIR are investigated using the code CIGALE to estimate physical parameters. We include far-UV (FUV) data from *GALEX*. We find that LBGs detected by SPIRE are high mass, luminous infrared galaxies. It appears that LBGs are located in a triangle-shaped region in the $A_{\rm FUV}$ vs. $Log L_{\rm FUV} = 0$ diagram limited by $A_{\rm FUV} = 0$ at the bottom and by a diagonal following the temporal evolution of the most massive galaxies from the bottom-right to the top-left of the diagram. This upper envelop can be used as upper limits for the UV dust attenuation as a function of $L_{\rm FUV}$. The limits of this region are well explained using a closed-box model, where the chemical evolution of galaxies produces metals, which in turn lead to higher dust attenuation when the galaxies age.

Keywords. galaxies: evolution — galaxies: formation — galaxies: high-redshift — infrared: galaxies — ultraviolet: galaxies

1. Introduction

The safest way to estimate the total star formation rates (SFRs) of galaxies is to consider the energy budget involving FUV and far-infrared (FIR) measurements (e.g., Buat *et al.* 1996). A small number of individual Lyman Break Galaxies (LBGs) have been detected in the FIR/submm range (e.g. Chapman *et al.* 2009, Siana *et al.* 2009). Since we have so little information, we need to observe these galaxies selected at lower redshift and examine their dust emission. Burgarella *et al.* (2007) detected dropout galaxies at $z \sim 1$ at $24 \, \mu$m with *Spitzer*. But, the dust luminosities were estimated from the rest frame $12 \, \mu$m flux density which is far from the peak of the dust emission, and therefore could easily have biased SFR values.

We observe in the FIR a sample of LBGs at $0.7 < z < 1.6$ (FUV dropouts) and at $1.6 < z < 2.8$ (near-UV or NUV dropouts). We use the SPIRE instrument Griffin *et al.* (2010) on *Herschel* Pilbratt *et al.* (2010) with observations from HerMES Oliver *et al.*

(2010)†. This is the first opportunity to estimate directly the dust luminosity (or upper limits) of unlensed LBGs from FIR data. More information can be found in Burgarella *et al.* (2011).

2. LBG samples

We cross-correlate the LBG samples defined in FUV and NUV using *GALEX* with the HerMES multi-wavelength catalog in GOODS-North from Roseboom *et al.* (2010) over $19' \times 12'$, i.e., $0.063 \deg^2$. Within this region we have 260 low-z LBGs and 1558 high-z in UV and among them, the final $0.7 < z < 1.6$ HerMES LBG sample contains 12 objects and the $1.6 < z < 2.8$ sample contains 1 object.

3. SED fitting

Dust luminosities, L_{IR}, and other parameters are estimated using CIGALE (Noll *et al.* 2009, http://www.oamp.fr/cigale) for the LBGs detected with SPIRE. This code performs a Bayesian analysis to estimate parameter by fitting models to the UV-to-submm SEDs. One can select among two single stellar population libraries and several IR models/templates. An AGN component can also be added to estimate the AGN fraction but f_{AGN} should only be used in a qualitative way above $f_{AGN} \sim 0.3$, since the number of AGN models used is limited. The parameters of the dust attenuation law can be modified and CIGALE allows for two separate stellar populations with a multiphase dust treatment. Individual SEDs with the best models selected by CIGALE are shown in Fig. 1 for the five LBGs with radio data and for one higher redshift ($z = 1.9$) LBG. Fig. 1 shows that CIGALE is able to fit the SEDs from the FUV to the radio successfully.

4. Dust attenuation of Lyman Break Galaxies

For the LBGs not detected by *Herschel*, we can estimate $\log(L_{IR})$ by using whatever limit provides the lowest value from the three SPIRE bands and therefore the lowest limit for the dust attenuation in the FUV. As above, L_{FUV} is estimated from rest-frame FUV measurements. Finally, from $\log(L_{IR}/L_{FUV})$ we can estimate A_{FUV}. Fig. 2 suggests that the maximum level of attenuation depends on L_{FUV} – the most UV-luminous LBGs yield a lower maximum A_{FUV} than less UV-luminous ones. This is true for upper limits as well as for detections. The two higher redshift lensed LBGs detected in FIR or in submm (the "Cosmic Eye", Siana *et al.* 2009 and cB58, Siana *et al.* 2008) also comply with this upper boundary, if we correct for the amplification. As do the two unlensed LBGs MM8 (Chapman *et al.* 2000) and MMD11 (Chapman & Casey 2009). Of course, most of the upper limits should populate the area below the observational limits but none would prevent us from detecting LBGs that would have larger FUV dust attenuations than the one suggested by the present data for a given L_{FUV}.

Reddy *et al.* (2010) find that UV-faint galaxies at $z \sim 2.5$ are less attenuated than UV-bright galaxies. However, their figure 13 shows that we cannot exclude that part of their detections are similar to ours, i.e. with A_{FUV} decreasing with increasing L_{FUV}. In Fig. 2 we overplot the mean relation from Reddy *et al.* (2010), modified to match our diagram using the Burgarella *et al.* (2005) calibration of $\log(L_{IR}/L_{FUV})$ into A_{FUV}. Carilli *et al.* (2008) and Ho *et al.* (2010) estimate the UV dust attenuation by comparing radio-based

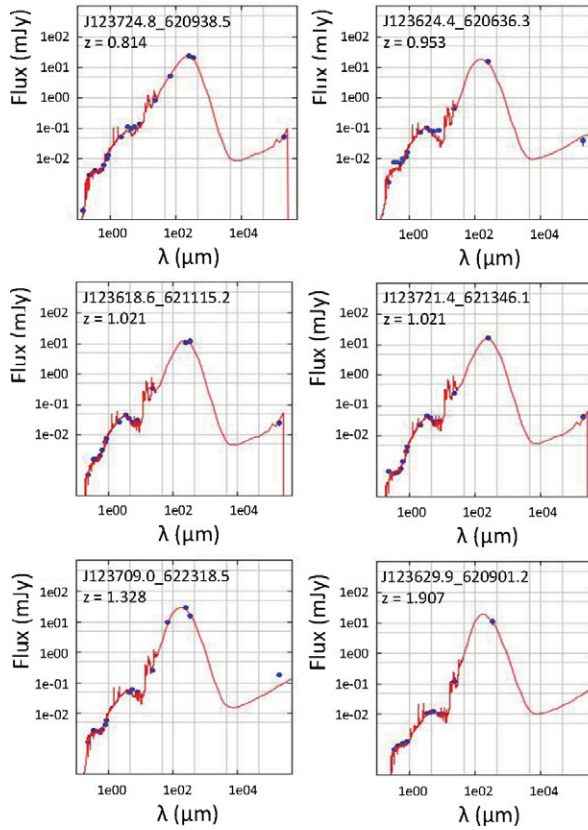† http://hermes.sussex.ac.uk

Figure 1. Observed spectral energy distributions of LBGs superimposed on best fit models (S_ν[mJy] vs. $\log \lambda$[μm]). Note that J123633.2+620834.9 very likely hosts an AGN, as suggested by the CIGALE SED fitting.

star formation rates to UV-based ones using a stacking analysis. We show in Fig. 2, the two points corresponding to different $\log L_{\rm FUV}$.

One explanation for this relates to the bimodal UV+IR luminosity function. Higher luminosities are expected to be rarer, which translates into a less populated upper-right part of Fig. 2.

To further understand the origin of this effect, we build a simple closed box model assuming several exponentially decreasing star formation histories $\Psi(t) = \Psi_0 e^{-t/\tau}$, with $\tau = 0.1$, 1 and 10 Gyr. We assume a mass of cold gas $M_{\rm gas}$ that forms stars following a Salpeter initial mass function, and thus produce heavy elements and dust (Burgarella *et al.* 2011). $M_{\rm gas}$ evolves as follows:

$$dM_{\rm gas}/dt = -\Psi(t) + E(t), \qquad (4.1)$$

where $E(t)$ is the mass ejected by stars at the end of their lifetime.

The models overplotted in Fig. 2 show that this simple closed box model follows the same trend as the LBGs in the diagram. The initial mass of gas is set to $\log(M_{\rm gas}/{\rm M}_\odot) = 10.5$ to explain the low redshift LBGs and $\log(M_{\rm gas}/{\rm M}_\odot) = 11.0$ (not plotted) for the high redshift LBGs.
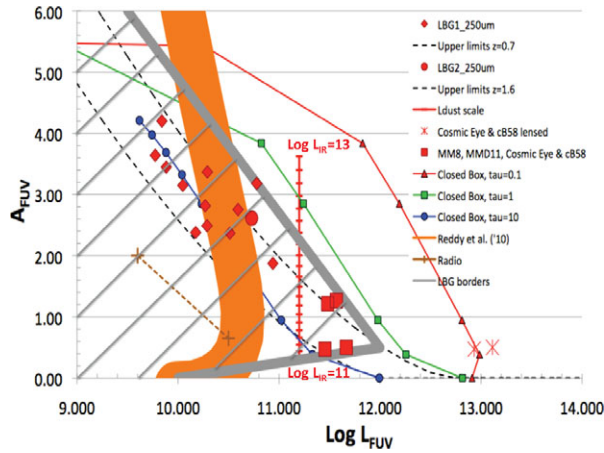
Figure 2. The relationship between attenuation and UV luminosity for LBGs. Green boxes are those detected up to $24\,\mu$m and red diamonds are those detected by *Herschel*. The two big red stars are the two high redshift LBGs (the Cosmic Eye and cB58) as observed, while the big red squares are the same sources after correcting for the amplification plus two unlensed ones. The blue dots, green boxes and red triangles are the closed-box models, plotted as a function of time (over 0–13 Gyrs) from the top-left to the lower right part of the diagram. The vertical scale provides the values of L_{IR} in steps of 0.1dex. The two crosses linked by a dashed line are radio-based measurements. Finally, the orange shaded area corresponds to the models of Reddy *et al.* (2010). The bottom line of this figure is that for our LBG sample, the maximum dust attenuation appears to decline with increasing L_{dust} that corresponds to the upper branch of Reddy *et al.* (2010).

References

Buat, V. & Xu, C., 1996, *A&A* 306, 61

Burgarella D., Buat V., Iglesias-Páramo, J., 2005, *MNRAS*, 360, 1413

Burgarella D., Buat V., Magdis G., & the HerMES team, 2011, *apJ*, (subm.)

Burgarella, D., Le Floc'h, E., & Takeuchi, T. T. 2007, *MNRAS*, 380, 986

Carilli C. L., *et al.*, 2008, *AJ*, 689, 883

Chapman S. C., Scott D., Steidel C. C., *et al.*, 2000, *MNRAS*, 319, 318

Chapman S. C., Casey ., 2009, *MNRAS* 398, 1615

Griffin, M., *et al. A&A* 518, L3

Ho I. T., *et al.*, 2010, *ApJ* 722, 1051

Noll S., Burgarella D., Giovannoli E., *et al.*, 2009, *A&A*, 507, 1793

Oliver S. J., et al., 2010, *A& A* , 518, L21

Reddy *et al.*, 2010, *ApJ*, 712, 1070

Pilbratt, *et al. A&A* 518, L1

Roseboom, I., *et al.* 2010, *MNRAS* (in press)

Siana B., *et al.*, 2009, *ApJ*, 698, 1273

Siana B., *et al.*, 2008, *ApJ*, 689, 59

Steidel C. C., Giavalisco M., Pettini M., Dickinson M., Adelberger K. L., 1996, *ApJ*, 462, L17